Supplementary material:
The EMEP MSC-W chemical transport model – technical description

D. Simpson[1,2], A. Benedictow[1], H. Berge[1], R. Bergström[3,4], L.D. Emberson[5], H. Fagerli[1], C.R. Flechard[6], G.D. Hayman[7], M. Gauss[1], J.E. Jonson[1], M.E. Jenkin[8], A. Nyíri[1], C. Richter[9], V.S. Semeena[1], S. Tsyro[1], J.-P. Tuovinen[10], Á. Valdebenito[1], & P. Wind[1,11]

1. EMEP MSC-W, Norwegian Meteorological Institute, Oslo, Norway
2. Dept. Earth & Space Science, Chalmers Univ. Technology, Gothenburg, Sweden
3. Dept. Chemistry, Univ. of Gothenburg, Gothenburg, Sweden
4. Swedish Meteorological and Hydrological Institute, Norrköping, Sweden
5. Stockholm Environment Institute, University of York, York, England
6. INRA, Agrocampus Ouest, UMR 1069 SAS, Rennes, France
7. Centre for Ecology and Hydrology, Wallingford, Oxfordshire, OX10 8BB, UK
8. Atmospheric Chemistry Services, Okehampton, Devon EX20 1FB, UK
9. Gesellschaft für Anlagen- und Reaktorsicherheit (GRS) mbH, Cologne, Germany
10. Finnish Meteorological Institute, P.O. Box 503, 00101 Helsinki, Finland
11. University of Tromsø, N-9037 Tromsø, Norway

S1 EMEP model revision history

Table S1: Summary of major EMEP MSC-W Eulerian model versions

Revision	Date	Main changes
rv1.7	Jul 2003	First 'unified' model, with both acidification and photochemical scheme, documented in Simpson et al. (2003).
rv2.5	Jul 2006	Used for IIASA (GAINS) source-receptor matrices. Changes in: N_2O_5 hydrolysis, EQSAM scheme for nitrate formation, PM-water added, ozone-flux outputs added, move to netcdf file format. Global modelling capability added.
rv3.0	Feb. 2008	**First public-domain release**. Included various small changes, e.g. to vegetation parameters, and numerous technical changes.
rv3.2		Improved deposition scheme, including co-deposition for SO_2, revised particle deposition scheme, daily snow instead of climatological. Code revisions for more flexible grids and global scale.
rv3.4	2009	Additional chemical schemes implemented, EmChem09 scheme developed, forecast model verions implemented.
rv3.6	2010	Boundary layer physics updates, convection routine added.
rv3.8	May 2011	**Second public-domain release**. Major revisions in: Aerosol dry deposition methodology, also revised sub-cloud scavenging; Biogenic VOC emission methods, rates; added cumulus scheme; ECMWF IFS model replaces PARLAM/HIRLAM NWPs as default meteorological driver;
rv3.9	Nov 2011	Major revisions: pH dependence of sulphate formation; added organic aerosol and SOA formation; use of daily FINNv1 forest fire module; changed temporal variations for sectors SNAP-1 (changing winter/summer ratios) and SNAP-2 (degree-days);
rv4β	March 2012	Soil NO emissions, preliminary road-dust production added, use of soil moisture index from ECMWF IFS fields. As used in Aas et al. (2012).
rv4.0	Summer 2012	**Third public-domain release**. Hourly emission variations replaced former day/night emission factors, more flexible handling of volcanic emissions, increased MMD of coarse nitrate to 3μm, small change in vertical distribution of emissions.

Many changes are continuous, for example there is an ongoing process to make the model more flexible with respect to meteorological drivers, chemical schemes, grid-projection, nesting and boundary conditions. The vertical coordinate scheme has been revised, and where possible global databases are being implemented (for example forest fires) for use by all model domains.

S2 Physical formulation and Numerics, additional information

The main paper has dealt with the physical and chemical formulation of the model. Here we address some of the numerical and computational details associated with the model structure.

S2.1 Convection

Numerical implementation of the convection scheme is as described in Jonson et al. (2010). We define the mass (per square meter) of a pollutant in the layer k as $\frac{\chi\,\Delta_k P}{g}$ where χ is the mass mixing ratio of a pollutant, $\Delta_k P$ is the pressure difference between the bottom and the top of the layer and g is the gravitational constant. The advantage of this formulation compared to using density times $\Delta\, z$, is that it is not dependent on a particular definition of the vertical coordinates.

We assume that the convective fluxes leaving the layer k through the top (cf. Fig. 3), F_k, are given by the meteorological driver. For **updrafts**, the process starts at surface (largest k). If $\Delta_k F = F_k - F_{k+1} > 0$, the pollutants are transported from the environment towards the cloud core (elevator). The mass of the pollutant removed from a grid cell and put into the core in layer k during time Δt, is given by $\chi_{grid}\,\Delta_k\, F\,\Delta t$, and the new mixing ratio becomes:

$$\chi_{grid}^{t+\Delta t} = \chi_{grid}^{t} - \chi_{grid}^{t}\frac{g\,\Delta_k F \Delta t}{\Delta_k P} \tag{1}$$

In this formulation $\Delta_k P$ is kept constant during the convection process. The mixing ratio of the pollutant in the cloud core becomes:

$$\chi_{core}^{t+\Delta t} = \chi_{core}^{t} + \chi_{grid}^{t}\frac{g\,\Delta_k F\,\Delta t}{\Delta_k P} \tag{2}$$

If mass is transported from the cloud core towards the grid cell, the proportion of pollutants removed from the core is given by $\frac{F_{k+1}-F_k}{F_{k+1}}$ and the new mixing ratios become

$$\chi_{grid}^{t+\Delta t} = \chi_{grid}^{t} + \chi_{core}^{t}\frac{F_{k+1} - F_k}{F_{k+1}} \tag{3}$$

$$\chi_{core}^{t+\Delta t} = \chi_{core}^{t} - \chi_{core}^{t}\frac{F_{k+1} - F_k}{F_{k+1}} \tag{4}$$

The pollutant in the core is then lifted to the next level:

$$\chi_{core(k-1)}^{t} = \chi_{core(k)}^{t+\Delta t}\frac{\Delta_{k+1} P}{\Delta_k P} \tag{5}$$

and the process is iterated until the top is reached.

A corresponding calculation for the downward fluxes is performed, starting from top and continuing down to the surface. After these detrainment and entrainment processes, the total mass of pollutants will be conserved, however there will be an imbalance between the quantity of air having entered and left the individual grid cells, because the large scale subsidence has

not yet been accounted for. In order to mimic the subsidence process, we perform the same procedure starting with χ =1 at all levels, which will account for the modelled transport of "pure air".

The mass in a specific level obtained, $\frac{\chi \Delta_k P}{g}$ will then give a measure of the excess or deficiency of air. The air masses are then redistributed along the vertical column. The levels are filled successively starting from above until the original masses are recovered. The pollutants follow the same pattern.

S2.2 Time-step control

The numerical solution of the advection requires that the so-called Courant number does not exceed 1. The Courant (or CFL) number CU_0 is defined as $\frac{\Delta t}{\Delta x}|u|$ where u is wind-speed. This ensures that material from one grid cell can not be advected beyond the borders of its downwind neighbour. For a variable horizontal grid size, this expression must be scaled by the map factor. If the Courant number is exceeded, the advection timestep is adjusted for different rows or columns where needed. The time step for the vertical advection can also be different from the time step in the horizontal directions, but all elementary time steps for the one dimensional advection have to be an integer fraction of Δt_{advec}. A too low Courant number will lead to an undesired increase in numerical diffusion and also an increase in CPU requirements.

For each row j and vertical level k, a maximum value for the time-step Δt in direction x is derived; the following expression is evaluated over all grid cells in the row:

$$\Delta t_{max}(j,k) \leq \frac{\Delta x}{max(m^2 \frac{u(i,j,k)}{m_y(i,j)}, 0) - min(m^2 \frac{u(i-1,j,k)}{m_y(i-1,j)}, 0)}$$

Where $m^2 = m_x(i,j)\ m_y(i,j)$, and m_x, m_y are map-factors (see also Sect. 2.2). Corresponding expressions for the y and vertical directions are used.

The time step is set to the same value for all cells in one single row in each horizontal direction, although they can be different for different rows and at different heights. See Wind et al. (2002) for further details of the time-step control system.

S2.3 Chemistry - numerical solution

As noted in Sect. 7.10, the chemical equations are solved using the TWOSTEP algorithm tested by Verwer et al. (1996) & Verwer and Simpson (1995). The formulae have however been re-arranged for greater computational efficiency (S. Unger. Pers. comm.), and so here we outline the algorithm as used in the model. Note that the notation here is different to that used by Verwer and Simpson (1995).

The algorithm used for the chemistry solutions are summarised below. From the main model, at the start (time t) of each advection time-step of length $\Delta \mathrm{t}_{\mathrm{advec}}$ (typically 20 mins), we have 3-d arrays ($C_m^{3D}(i,j,k)$) of the chemical concentrations (in molecules cm^{-3}) of each species m, and of the chemical tendency, D_m (see below). Within one $\Delta \mathrm{t}_{\mathrm{advec}}$ we use a number $\mathrm{N}_{\mathrm{chem}}$ of chemical time-steps, of (uneven) width $\Delta t(n)$, where n = 1 ... $\mathrm{N}_{\mathrm{chem}}$ (see below). We will use the notation $t(n) = t + \Delta t(1) + \ldots + \Delta t(n)$. The scheme uses two values of concentrations, $\mathrm{C}_{\mathrm{m}}^{\mathrm{t(n-2)}}$ and $\mathrm{C}_{\mathrm{m}}^{\mathrm{t(n-1)}}$, to derive the next value $\mathrm{C}_{\mathrm{m}}^{\mathrm{t(n)}}$.

1.Initialise time-step

$\mathrm{C}_{\mathrm{m}}^{\mathrm{t(0)}} = C_m^{3D}(i,j,k)$	start with concentrations from 3-D fields at time t
$\mathrm{C}_{\mathrm{m}}^{\mathrm{t(-1)}} = \mathrm{C}_{\mathrm{m}}^{\mathrm{t(0)}} - 1.5\ D_m(i,j,k)\tau(1)$	Estimate based upon chemical tendency only. (D_m and τ defined below, D_m=0 when program starts).

2. Integration loop

For each chemical time-step (for n = 1 ... $\mathrm{N}_{\mathrm{chem}}$) we then do:

$\mathrm{C}_{\mathrm{m}}^{*} = \alpha(n)\mathrm{C}_{\mathrm{m}}^{\mathrm{t(n-1)}} - \beta(n)\mathrm{C}_{\mathrm{m}}^{\mathrm{t(n-2)}}$	help variable
$\mathrm{C}_{\mathrm{m}}^{\mathrm{t(n)}} = \mathrm{C}_{\mathrm{m}}^{\mathrm{t(n-1)}} + (\mathrm{C}_{\mathrm{m}}^{\mathrm{t(n-1)}} - \mathrm{C}_{\mathrm{m}}^{\mathrm{t(n-2)}})\gamma(n)$	First guess of new concs

For the general time-step n, coefficients α, β, γ, τ are calculated with:
$\theta(n) = \Delta t(n-1)/\Delta t(n)$ (for n=1, we use θ(1)=1)
$\beta(n) = 1/(\theta(n)^2 + 2\theta(n))$
$\alpha(n) = (\theta(n)+1)^2\beta(n)$
$\tau(n) = (\theta(n)+1)/(\theta(n)+2))\ \Delta t(n)$
$\gamma(n) = 1/\theta(n)$

2a. Calculation of $\mathrm{C}_{\mathrm{m}}^{\mathrm{t(n)}}$

Following Verwer and Simpson (1995), a Gauss-Seidel integration procedure is then used, where for each species m, the production rate P_m, loss-rate L_m, and then the updated concentrations $\mathrm{C}_{\mathrm{m}}^{\mathrm{t(n)}}$ are calculated in turn. The updated concentration for the iteration is then obtained using a Padé approximation of the second order backward difference formula:

$$\mathrm{C_m^{t(n)}} = \frac{\mathrm{C_m^*} + \tau(n) P_m}{1 + \tau(n) L_m} \tag{6}$$

At each stage the the latest values of concentrations are used for all reactants. Step 2a, running through all species and using Eqn. 6 is iterated a number of times (from 1 to 3, see below). We then save the chemical tendencies and return the new concentrations of advected species to the 3-D fields:

$D_m = (\mathrm{C_m^{t(n)}} - C_m^{3D}(i,j,k))/\Delta t_{\mathrm{advec}}$
$C_m^{3D}(i,j,k) = \mathrm{C_m^{t(n)}}$

At present, with an advection time-step $\Delta \mathrm{t_{advec}}$ of 20 minutes (1200 s) the algorithm starts with five successive timesteps of $\Delta \mathrm{t_{chem}}$ =20 s followed by seven larger timesteps of just under 160 s. Compared with a fixed timestep, increasing timesteps has been found more efficient, since at the start of the process the system is further away from a steady-state situation. This scheme improves with iteration. In the 4 layers near the ground, where emission and usually reaction tendencies are highest, we perform 3 iterations each timestep. Above this, 2 iterations are performed, except for the uppermost 6 layers where 1 iteration is used.

S2.4 Parallel structure and CPU requirements

In order to produce results covering several years and several different situations, the model requires large computer resources. The program code is written in Fortran 90/95. The structure of the program is designed to allow for efficient parallelization on a system with distributed memory.

The horizontal grid is divided into a number of subdomains and each subdomain is assigned to a processor. Each processor holds only the data for its own subdomain. Because of this structure, the communication between the processors is kept to a minimum.

Still the advection routines fundamentally require information to be passed between processors. An additional limitation of the level of parallellity which can be achieved is that much input/output is currently done on one processor, and thus requires information to be passed between the processors. The meteorological data for example is stored on disc and has to be read serially and distributed to all the nodes. Also the writing of results cannot yet be done entirely in parallel. Further details on the parallel architecture of the code can be found in Skålin et al. (1995).

The most CPU demanding part of the program is the chemistry module, because of the large number of chemical components and reactions. The chemical reactions have to be described for all the grid-cells and with a small time scales. However the chemistry is local and is therefore perfectly suited for parallelization. The deposition and wet scavenging processes have only vertical data dependencies and will therefore also parallelize effectively with the partitioning adopted in the program.

A typical run covering one year in a 159x133 grid will require less than four real time hours (128 CPU hours) on 32 processors. The typical relative CPU usage of the different part of the

program are: Chemistry 60% , Advection 10%, Meteorology and input/output 10%, Synchronisation between nodes 10%, others 10%. For larger grids more processors are used; the model has been tested for up to 1024 CPUs and scales well.

S3 Derivation of 'missing' meteorological parameters

As noted in Sect. 3 the EMEP model has to have systems for deriving parameters when missing, or can do without some meteorological fields. Two important cases are for 3-D precipitation and vertical wind-speed.

S3.1 3-D precipitation fields

When precipitation data are not available as a three dimensional fields, they are derived from surface precipitation. The height of the precipitation release is derived either from cloud water, if available, or humidity if cloud water is not available. The height of the precipitation is then defined as the highest altitude above the lowest level, where the cloud water is larger than a threshold taken as 1.0×10^{-7} kg water per kg air (or when the relative humidity is larger than 0.85 in case cloud water is not available). Precipitations are only defined in areas where surface precipitations occur. The intensity of the precipitation is assumed constant over all heights were they are non-zero.

S3.2 Vertical wind speed

When the vertical wind speed $\dot{\sigma}$ is not available, it is derived from the continuity equation (see also Travnikov et al. (2009)) using

$$(\dot{\sigma})_{k+\frac{1}{2}} \left(P_S - P_{top}\right) = \sigma_{k+\frac{1}{2}} \sum_{r=Surf}^{top} \vec{\nabla} \left(\vec{V}_r \, \Delta P_r\right) - \sum_{r=k}^{top} \vec{\nabla} \left(\vec{V}_r \, \Delta P_r\right) \tag{7}$$

Use of this formula directly ensures that $(\dot{\sigma})_S = 0$ at surface since $\sigma_S = 1$, and $(\dot{\sigma})_{top} = 0$ at top since $\sigma_{top} = 0$.

S4 Emissions

S4.1 Annual totals

Table S2: Emissions (Gg a^{-1}) for the year 2008 used in the EMEP model.

	Anthropogenic						Biogenic‡		
	SOx (as SO_2)	NOx (as NO_2)	NMVOC	NH_3	PMf	PMc	soil-NO (as NO_2)	Isop.	MT
Albania	37	29	32	24	14	4.0	3.2	9.2	32
Armenia	26	24	41	17	0.3	0.5	–	–	0.1
Austria	22	204	150	63	21	16	2.5	12	35
Azerbaijan	91	91	238	53	3.8	0.6	–	–	0.4
Belarus	84	189	387	147	53	13	4.5	34	61
Belgium	97	239	118	67	20	8.1	–	5.0	4.0
Bosnia	431	51	43	17	19	24	1.8	13	18
Bulgaria	569	141	84	62	31	28	9.0	41	94
Croatia	58	85	109	38	11	4.7	1.1	17	20
Cyprus	23	20	12	5.3	2.8	1.5	–	–	0.5
Czech	174	261	166	58	21	14	1.3	14	22
Denmark	19	150	96	78	28	6.2	–	4.4	5.7
Estonia	69	36	38	11	20	5.4	–	2.8	3.3
Finland	70	168	118	38	38	14	1.4	35	41
France	344	1194	957	672	267	118	2.9	49	68
Georgia	22	46	231	26	1.9	0.3	–	–	0.3
Germany	490	1418	1017	568	110	85	4.3	56	99
Greece	444	394	228	65	63	37	9.7	25	112
Hungary	88	183	141	69	23	15	2.4	22	31
Iceland	74	24	5.7	3.0	0.5	0.1	–	1.0	4.0
Ireland	46	110	51	107	9.5	5.2	–	–	0.2
Italy	283	1057	1194	409	173	31	11	65	149
Kazakstan	381	171	155	573	25	14	11	61	149
Kyrgyzstan	26	63	25	27	11	9.3	–	–	0.1
Latvia	4.7	34	74	16	26	6.3	0.4	9.9	12
Lithuania	27	55	66	29	9.5	2.6	0.5	7.5	13
Luxembourg	2.3	50	10	4.7	2.2	0.9	–	1.3	0.9
FYR Macedonia	114	37	28	7.0	8.8	9.5	1.7	4.2	18
Malta	11	9.0	3.0	1.5	1.4	0.8	–	0.5	1.2
Moldova	7.5	32	35	26	6.2	3.8	2.6	10	26
Montenegro	15	9.5	10	3.2	5.5	4.2	0.8	2.7	8.4
Netherlands	51	309	162	127	17	14	–	0.3	1.0
Norway	20	189	154	23	46	6.3	0.2	28	35
Poland	995	832	641	285	122	125	4.8	31	72
Portugal	108	211	192	47	59	26	–	9.4	9.7
Romania	566	287	465	187	123	21	15	73	182
Russia	1575	3789	2566	599	384	216	71	457	978
Serbia	265	194	133	89	25	16	6.7	30	61
Slovakia	69	94	67	25	28	3.7	1.2	3.0	20
Slovenia	13	53	33	18	13	3.1	–	0.6	1.4
Spain	513	1061	730	354	82	35	1.7	44	65
Sweden	30	158	196	52	28	12	0.3	27	33
Switzerland	14	83	93	65	10.0	11	0.5	6.0	6.4
Turkey	1041	860	1000	409	247	93	0.6	5.2	25
UK	491	1317	922	283	73	52	–	11	13
Ukraine	1386	825	311	206	276	185	37	212	419

Notes: Data from anthropogenic sources were updated in 2012 (see `www.ceip.at/webdab-emission-database`); '–' indicates values less than 0.1 Gg a^{-1}.

‡ Emissions from biogenic sources are estimated from gridded data using country area fractions only. Values for small countries are very approximate;

S4.2 Spatial distribution

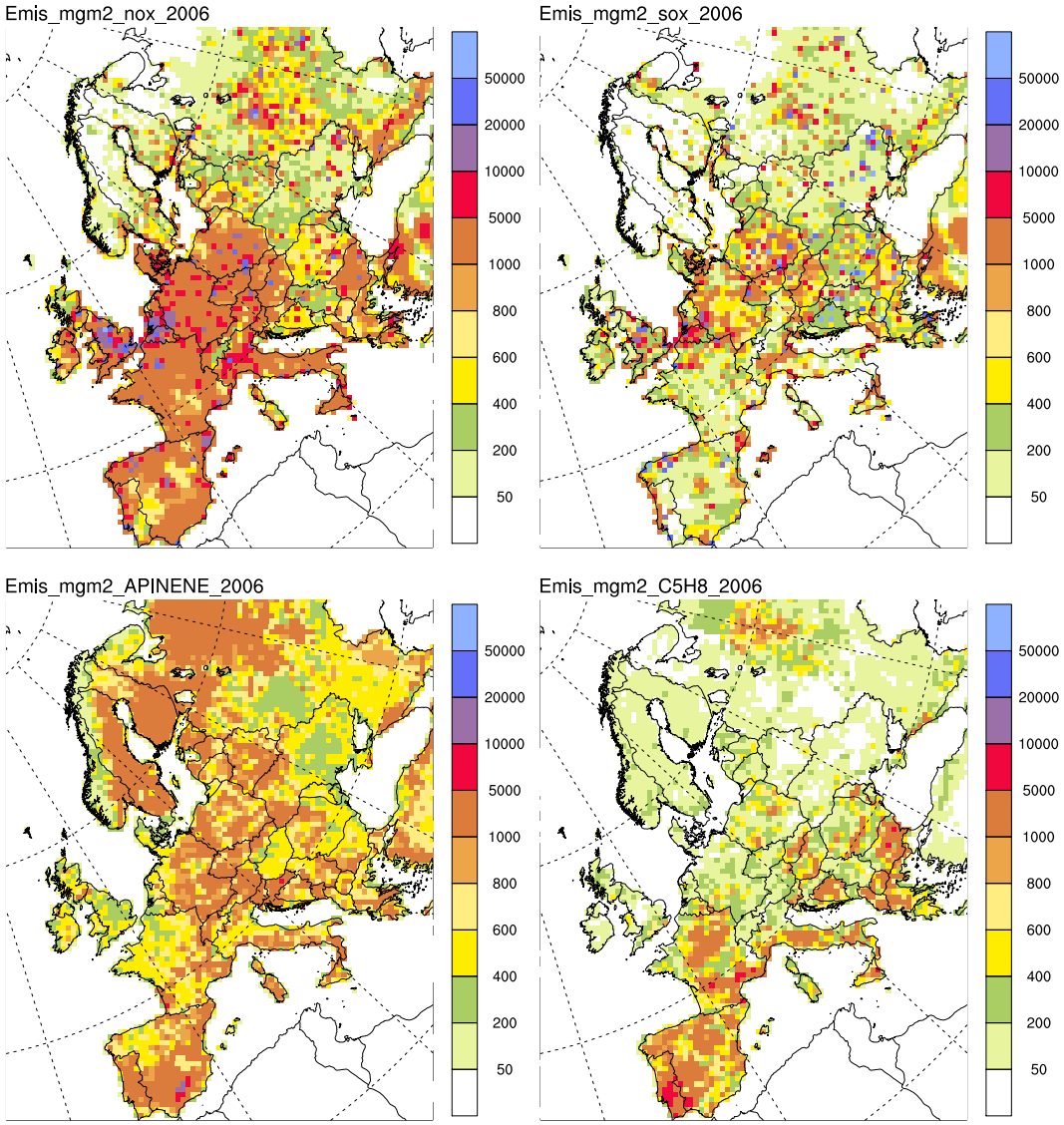

Figure S1: Emissions of NO_x, SO_2, monoterpenes (surrogate APINENE) and isoprene in the EMEP grid for the year 2006. Units: mg m^{-2}.

S4.3 Anthropogenic emissions, additional Tables

Table S3: Vertical distribution of anthropogenic emissions: percentage of each SNAP emission sector allocated to the vertical layers of the EMEP model (given as heights of layers, in m, for a standard atmosphere).

No.	Sources	Height of Emission Layer (m)					
		0-92	92-184	184-324	324-522	522-781	781-1106
1	Combustion in energy and transformation industries			15	40	30	15
2	Non-industrial combustion plants	100[(a)]	0[(a)]				
3	Combustion in manufacturing industry	10	10	15	30	30	5
4	Production processes	90	10				
5	Extraction and distribution of fossil fuels and geothermal energy	90	10				
6	Solvents and other product use	100					
7	Road transport	100					
8	Other mobile sources and machinery	100					
9	Waste treatment and disposal	10	15	40	35		
10	Agriculture	100					

Notes: (a) Up to version rv4β SNAP-2 was split 90% into the lowest layer, then 10% in the next lowest.

Table S4: Day[(a)] and night factors applied to anthropogenic emissions in code versions up to rv4β. In the latest (rv4) model version, hourly emission factors are applied, depending on day-of-week and SNAP sector. (These new factors were provided by INERIS, B. Bessagnet, pers.comm.)

SNAP:	1	2	3	4	5	6	7	8[(b)]	9	10
Day	1.0	1.2	1.2	1.5	1.0	1.5	1.5	1.2	1.0	1.4
Night	1.0	0.8	0.8	1.0	1.0	0.5	0.5	0.8	1.0	0.6

Notes: (a) Defined as between 7am and 6pm local time; (b) SNAP8 covers a range of non-road traffic soures, including shipping. Emissions from international shipping assumed constant over 24 h.

Table S5: Default speciation of VOC emissions: Percentage (by mass) of each emissions (SNAP) sector allocated to model species. Data derived from Passant (2002), see also Hayman et al. (2012).

SNAP	C2H6	NC4H10	C2H4	C3H6	C5H8	OXYL	CH3OH	C2H5OH	HCHO	CH3CHO	MEK	GLYOX	MGLYOX	UNREAC
1	12.559	14.836	2.406	4.376	0.000	9.479	0.000	0.000	55.691	0.034	0.620	0.000	0.000	0.000
2	12.589	39.790	8.174	10.767	0.000	18.632	0.000	3.912	5.586	0.207	0.089	0.000	0.000	0.255
3	4.996	35.610	9.044	2.089	0.000	18.323	0.561	3.034	24.134	0.059	1.347	0.000	0.000	0.805
4	2.652	34.519	5.458	4.257	0.142	13.380	1.176	31.414	0.077	0.978	1.608	0.000	0.000	4.337
5	17.842	79.895	0.018	1.569	0.008	0.505	0.000	0.000	0.078	0.000	0.000	0.000	0.000	0.085
6	0.444	44.052	0.244	0.678	0.008	17.904	6.101	16.416	0.011	0.000	9.965	0.000	0.000	4.176
7	4.832	36.698	6.796	10.896	0.000	35.051	0.000	0.000	2.700	2.606	0.421	0.000	0.000	0.000
8	3.775	47.416	6.636	10.608	0.000	24.676	0.000	0.000	3.115	3.261	0.235	0.146	0.117	0.014
9	25.718	36.778	5.237	1.830	1.153	7.881	0.427	2.439	16.060	0.000	0.093	0.000	0.000	2.383
10	0.000	0.000	0.000	0.000	0.000	0.000	0.000	0.000	0.000	0.000	0.000	0.000	0.000	100.000

Notes: For definition of model species (e.g. MEK, OXYL) see Table S5, Table S5, except for non-reacting species here (UNREAC) which are excluded from the calculations.

Table S6: Default speciation of coarse (2.5–10μm) PM emissions: Percentage (by mass) of each emission (SNAP) sector allocated to organic matter (OM), elemental carbon (EC) and remaining coarse primary particulate matter (REMPPM_c).

SNAP	OM	EC$^{(a)}$	REMPPM_c
1	1	5	94
2	50	20	30
3	5	10	85
4	5	5	90
5	5	5	90
6	10	40	50
7	40	30	30
8	45	45	10
9	40	30	30
10	40	20	40
11	70	0	30

(a) EC further split into 80% ECnew_f, 20% ECage_f. If explicit wood-burning emissions available, a 50:50 split is assumed between ECnew_f, ECage_f.

S4.4 Foliar emissions, additional Tables

Table S7: Forest-specific biomass density and emission factors (leaf-level).

EMEP Code (Λ)	Species (λ)	Common name	Biomass density (D) $\mathrm{g m^{-2}}$	Emission factors ($\mu \mathrm{g\,g^{-1} h^{-1}}$) Isoprene $\varepsilon_{\Lambda_{c,iso}}$	Monoterpenes $\varepsilon_{\Lambda_{c,mtl}}$	$\varepsilon_{\Lambda_{c,mtp}}$
CF	Abies alba	Silver Fir	1200	0	0	1
CF	Abies bori.	Bulgarian Fir	1200	10	0	3
CF	Abies	other Fir	1200	0	0	3
DF	Acer		320	0	2	0
DF	Alnus glutinosa	Common Alder	320	0.2	3	0
DF	Alnus	other Alder	320	0	1.5	0
BF	Arbutus		300	0.1	0.1	0
DF	Betula	Birch	320	0	0	3
NF	Buxus Semi.	Common box	320	10	0	0.2
DF	Carpinus bet.	European Hornbeam	320	0	0	0.7
DF	Carpinus	other Hornbeam	320	0	1	0.5
DF	Castanea	Chestnut - all	320	0	10	0
NF	Cedrus	Cedar	700	0	0	0.7
DF	Cercis sil.	Judas tree	320	0	0	0
NF	Ceratonia silq	Carob tree	320	0	0	0
DF	Corylus avel.	Hazel tree	320	0	0	0
NF	Cupressus	Cypress	700	0.1	0	0.7
NF	Erica arbor.	Tree Heath	100	10	0	3
NF	Erica	other Erica	150	0	0	0
NF	Eucalyptus	Eucalyptus	400	35	0	3
DF	Fagus	Beech	320	0	10	0

Cont. on next page

Notes: See Sect. 6.6 for explanation of rates and algorithms.

Table S7: cont.

Λ	λ		D	$\varepsilon_{\Lambda_{c,iso}}$	$\varepsilon_{\Lambda_{c,mtl}}$	$\varepsilon_{\Lambda_{c,mtp}}$
DF	Fraxinus	Ash (all)	320	0	0	0
NF	Ilex aqui.	Holly	320	0	0	0
BF	Juglans	Walnut	320	0	0	1
NF	Juniperus	Juniper	700	0	0	1
DF	Larix kaemp.		300	0	0	8
DF	Larix	Larch (other)	300	0	0	5
NF	Laurus nobilus	Laurel	500	0	0	0
DF	malus domestica	Apple	320	0	0	0
NF	Olea	Olive	200	0	0.2	0
DF	Ostrya Carp.	Hop Hornbeam	320	0	0	0
NF	Philyrea latifolia	Green Olive	300	0	0.4	0.1
CF	Picea abies	Norway spruce	1400	1	0.5	1
CF	Picea sitch.	Sitka spruce	1400	5	0	3
CF	Picea	Other spruce	1400	1	0.5	1
NF	Pinus pinaster	Maritime pine	700	0	0	1.5
NF	Pinus pinea	Stone pine	700	0	4	2
CF	Pinus sylvestris	Scots pine	700	0.1	1	2
CF	Pinus uncinata	Mountain pine	700	0.1	0	3
NF	Pinus radiata	Monterey pine	700	0	1	1
CF	Pinus - other	Other pine	700	0	0	3
BF	Pistacia lent.		320	0	0	0.7
BF	Pistacia tere.		320	0	0.5	0
DF	Platanus orientali	Oriental plane	320	50	0	3
DF	Populus alba		320	60	1	0
DF	Populus tremula		320	45	3	0
DF	Populus	Other Poplar	320	45	1	0
DF	Prunus		300	0	0.2	0
CF	Psuedotsuga menz.	Douglas Fir	1000	1	0	3

Cont. on next page

Table S7: cont.

Λ	λ		D	$\varepsilon_{\Lambda_{c,iso}}$	$\varepsilon_{\Lambda_{c,mtl}}$	$\varepsilon_{\Lambda_{c,mtp}}$
DF	Pyrus comm.	European pear	320	0	0	0
DF	Quercus cerr.	Turkey oak	320	0.1	1	0.5
BF	Quercus cocc.	Kermes oak	320	0.1	10	0
DF	Quercus fagi.	Portugese oak	320	100	0.5	0
DF	Quercus frai.	Hungarian (Italian) oak	320	100	0	0
BF	Quercus fruc.		320	0.1	20	0
BF	Quercus ilex.	Holm (Holly) Oak	500	0.1	30	0
DF	Quercus macr.	Caucasian (Persian)	320	0.2	0	0.5
DF	Quercus petr.	Sessile oak	320	45	0.5	0
DF	Quercus pube.	Downy oak	320	80	0.2	0
DF	Quercus pyre.	Pyerenean oak	320	60	0.5	0
DF	Quercus robu.	Pendunculate (English) oak	320	80	0.2	0.2
BF	Quercus rotu.		320	0.2	15	0
DF	Quercus rubra	N. Red Oak	320	60	1	0
BF	Quercus sube.	Cork oak	500	0.2	20	0
BF	Quercus troj.	Macedonian oak	320	0.2	0.2	0
DF	Robinia pseu.	Locust	320	20	3	0
DF	Salix	Willow	150	20	0	1
DF	Sorbus	Whitebeam	320	0	0	0
DF	Taxus baccata	Yew	320	0	0	0
CF	Thuya sp.		320	0	0	0.5
DF	Tila sp.	Lime/Linden	320	0	0	0
CF	Tsuga sp.	Hemlock	320	0.1	0	1.5
DF	Ulmus sp.	Elm	320	0.1	0	0.1
DF	Other broadleaf		320	5	0	0.2
CF	Other coniferous		500	1	1	2

S4.5 Sea-salt, equations

The parameterisation scheme for calculating sea salt generation has been presented and discussed in Tsyro et al. (2011), so here we present just the basic equations for the two source functions. The first one is a source function constructed by Monahan et al. (1986):

$$\frac{dF}{d\,r_{80}} = 1.373\; V_{10}^{3.41}\; r_{80}^{-3}\left(1 + 0.057\, r_{80}^{1.05}\right) \times 10^{1.19\;\exp(-B^2)} \tag{8}$$

where $d\,F/d\,r_{80}$ is the rate of sea salt droplet generation per unit area of sea surface and per increment of the aerosol radius r_{80} at 80 % relative humidity (see below), V_{10} is the wind speed at 10 m, and $B = (0.380 - \log(r_{80})/0.650$.

The second scheme is a source function from the work of Mårtensson et al. (2003), which is formulated for sea water salinity of 33 ‰:

$$\frac{dF}{d\log D_{\rm d}} = 3.84 \cdot 10^{-6}\,(A_k T_{\rm w} + B_k) \cdot V_{10}^{3.41} \tag{9}$$

where $d\,F/d\,(\log D_{\rm d})$ is the flux of sea salt particle per unit area of the whitecap cover and per increment of ($\log\ D_{\rm d}$), $D_{\rm d}$ is the dry diameter, $T_{\rm w}$ is the temperature of sea water, equal to Sea Surface Temperature (SST), or to T_2 if SST is unavailable from the NWP model, and A_k and B_k are the parameters describing the dependence of sea salt flux on the aerosol size:

$$\begin{aligned} A_k &= c_4 D_{\rm d}^4 + c_3 D_{\rm d}^3 + c_2 D_{\rm d}^2 + c_1 D_{\rm d} + c_0 \\ B_k &= d_4 D_{\rm d}^4 + d_3 D_{\rm d}^3 + d_2 D_{\rm d}^2 + d_1 D_{\rm d} + d_0 \end{aligned} \tag{10}$$

and the empirical coefficient c_i and d_i are tabulated according to Mårtensson et al. (2003).

The relationship between the dry radius $r_{\rm d}$ and radius at the supersaturation S=0.8 (for relative humidity of 80 %) for sea salt aerosols is expressed through an empirical formula, as suggested in Gong et al. (1997):

$$r_{80} = \left(\frac{0.7674 r_{\rm d}^{3.079}}{2.573\ 10^{-11}\ r_{\rm d}^{-1.424} - \log_{10} S} + r_{\rm d}^3\right)^{1/3} \tag{11}$$

First, sea aerosol fluxes are calculated for ten size bins, using Mårtensson et al. (2003) parameterisation for the first six bins (up to dry diameter of 1.25 μm) and Monahan et al. (1986) scheme for the larger sizes. The generated sea salt aerosols are aggregated in two size fractions, i.e. the fine fraction with (Mass Median Diameter MMD = 0.33 μm) and the coarse fraction (MMD = 4.0 μm). The total production rates of the fine and coarse sea salt are found by integrating the size resolved fluxes over respective size intervals. Finally, the generated sea salt aerosols are assumed to be instantaneously mixed within the model lowest layer (approximately 90 m height) at each time step.

S5 Default chemical mechanism, EmChem09

We give below the gas and inorganic particle phase chemical mechanism. (For comments on secondary organic aerosol, see Sect. 7.9.)

Table S8: Listing of non-advected (short-lived) species used in default EmChem09 chemical scheme.

Model species	Formula
OD	O
OP	O
OH	OH
HO2	HO_2
CH3O2	CH_3O_2
C2H5O2	$C_2H_5O_2$
SECC4H9O2	sec-$C_4H_9O_2$
ISRO2	$HOC_5H_8O_2$
ETRO2	$CH_2O_2CH_2OH$
PRRO2	$CH_3CHO_2CH_2OH$
OXYO2	$C_8H_{11}O_3O_2$
MEKO2	$CH_3COCHO_2CH_3$
MALO2	$CH_3COCH(OH)CH(O_2)CHO$
MVKO2	$HOCH_2CH(OO)C(CH_3)$=O
MACRO2	O=$CHC(O_2)(CH_3)CH_2OH$
MACO3	$CH_2C(CH_3)C(=O)O_2$

Table S9: Listing of advected core species used in default EmChem09 chemical scheme.

Model species	Formula	DRY†	WET†
O3	O_3	O3	
NO	NO		
NO2	NO_2	NO2	
PAN	$CH_3COO_2NO_2$	PAN	
MPAN	$CH_2CH(CH_3)COO_2NO_2$	PAN	
NO3	NO_3		
N2O5	N_2O_5		
ISONO3	$NO_3C_5H_8O$		
HNO3	HNO_3	HNO3	HNO3
HONO	HONO	HNO2	HNO3
H2	H_2		
CO	CO		
CH4	CH_4		
SO2	SO_2	SO2	SO2
SO4	SO_4^{2-}	PMfS	SO4
NH3	NH_3	NH3	NH3
NO3_f	NO_3^-	PMfN	PMf
NO3_c	NO_3^-	PMc	PMc
NH4_f	NH_4^+	PMfN	PMf
CH3COO2	CH_3COO_2		
MACR	CH_2=CCH_3CHO		
ISNI	generic		
ISNIR	generic		
GLYOX	HCOHCO		
MGLYOX	CH_3COCHO		
MAL	CH_3COCH=$CHCHO$	ALD	
MEK	$CH_3COC_2H_5$		
MVK	$CH_3C(=O)CH$=CH_2		
HCHO	HCHO	HCHO	HCHO

Table gives: Model species – name as used in code, Formula – chemical formula when needed by GenChem (sometimes omitted), DRY – species from which dry-deposition rates calculated, WET – species from which wet-deposition rates calculated. Suffix _f, _c refer to fine and coarse mode aerosol species.

† Notation for gaseous compounds relates to *Wesely, 1989*, although methodology differs. PMf, PMc indicate particle deposition rates for fine and coarse aerosols, for sulphate-like (PMfS) or fine-nitrate-like (PMfN) compounds.

The Table omits the species involved in the SOA mechanism, since these vary very much with mechanism, and also do not affect the core chemstry.

Table S9: cont.

Model species	Formula	DRY	WET
CH3CHO	CH_3CHO	ALD	
C2H6	C_2H_6		
NC4H10	nC_4H_{10}		
C2H4	C_2H_4		
C3H6	C_3H_6		
OXYL	o-$C_6H_4(CH_3)CH_3$		
C5H8	CH_2=HCC=CH_2CH_3		
CH3O2H	CH_3O_2H	ROOH	
C2H5OOH	C_2H_5OOH	ROOH	
BURO2H	$secC_4H_9O_2H$		
ETRO2H	$CH_2O_2HCH_2OH$		
PRRO2H	$CH_3CHO_2HCH_2OH$		
OXYO2H	$C_8H_{11}O_3O_2H$		
MEKO2H	$CH_3COCHO_2HCH_3$		
MALO2H	$CH_3COCHOHCHO_2CHO$		
MVKO2H	$HOCH_2CH(O_2H)C(CH_3)$=O		
MACROOH	O=$CHC(CH_3)(OOH)CH_2OH$		
MACO3H	CH_2=$C(CH_3)C$(=O)OOH		
MACO2H	CH_2=$C(CH_3)C$(=O)OH		
ISRO2H	$HOC_5H_8O_2H$		
H2O2	H_2O_2	SO2	H2O2
CH3COO2H	CH_3COO_2H		
ISONO3H	$NO_3C_5H_8O_2H$		
ISNIRH	generic		
CH3OH	CH_3OH		
C2H5OH	C_2H_5OH		
ACETOL	CH_3COCH_2OH	ALD	

Table S10: Listing of some optional, inert and tracer species

Model species	Formula	DRY†	WET†	Comments
APINENE	$C_{10}H_{16}$			Used if SOA scheme
ECnew_f		PMfS	PMecf	Fresh (hydrophibic) EC
ECage_f		PMfS	PMf	Aged (mixed, and hydrophillic) EC
SeaSalt_f		PMfS	PMssf	
SeaSalt_c		PMc	PMssc	
Dust_f		PMfS	PMf	
Dust_c		PMc	PMc	
REMPPM_f		PMfS	PMf	'remaining' primary particulate matter, fine-mode (excluding OM, EC)
REMPPM_c		PMc	PMc	As REMPPM_f, coarse mode
PPM25_FIRE		PMfS	PMf	Fire tracer
CO_FIRE	CO			Fire tracer
Rn222				Radon isotope tracer
Pb210		PMfS	PMf	Product from radon decay

Notes: Suffix _f, _c refer to fine and coarse mode aerosol species.

Table S11: Default Chemical Mechanism of EMEP model, EmChem09. For Notes, see end of Table

N	Rate coefficient	Reaction
Inorganic chemistry		
IN-1	$(6.0 \times 10^{-34}$ O2 ...	OP + O2 + M ⇒ O3
	... + 5.6×10^{-34} N2) × O2 × $(T/300)^{-2.6}$	
IN-2	$1.8{\times}10^{-11} \exp(107/T) \times$ N2	OD + N2 ⇒ OP
IN-3	$3.2 \times 10^{-11} \exp(67/T) \times$ O2	OD + O2 ⇒ OP
IN-4	2.2×10^{-10} H2O	OD + H2O ⇒ 2. OH
IN-5	$1.4 \times 10^{-12} \exp(-1310/T)$	O3 + NO ⇒ NO2 + O2
IN-6	$1.4 \times 10^{-13} \exp(-2470/T)$	O3 + NO2 ⇒ NO3 + O2
IN-7	$1.7 \times 10^{-12} \exp(-940/T)$	O3 + OH ⇒ HO2 + O2
IN-8	$2.03 \times 10^{-16} \times$ ...	O3 + HO2 ⇒ OH + 2 O2
	$\ldots (300/T)^{-4.57} \exp(693/T)$	
IN-9	$1.8 \times 10^{-11} \exp(110/T)$	NO + NO3 ⇒ NO2 + NO2
IN-10	$3.6 \times 10^{-12} \exp(270/T)$	NO + HO2 ⇒ NO2 + OH
IN-11	$4.5 \times 10^{-14} \exp(-1260/T)$	NO2 + NO3 ⇒ NO + NO2
IN-12	$4.8 \times 10^{-11} \exp(250/T)$	OH + HO2 ⇒ H2O + O2
IN-13	$2.9 \times 10^{-12} \exp(-160/T)$	OH + H2O2 ⇒ HO2 + H2O
IN-14	$7.7 \times 10^{-12} \exp(-2100/T)$	OH + H2 ⇒ HO2 + H2O
IN-15	$k_{OH+HNO3}$	OH + HNO3 ⇒ NO3 + H2O
IN-16	$k_{HO2+HO2}$	HO2 + HO2 ⇒ H2O2
IN-17	$2.5 \times 10^{-12} \exp(-260/T)$	OH + HONO ⇒ NO2
IN-18	k_{N2O5} (a)	N2O5 ⇒ 2. HNO3
IN-19	k_{aero}	HNO3 ⇒ NO3_c
IN-20	kt_{NO+OP}	OP + NO + M ⇒ NO2
IN-21	$kt_{NO2+NO3}$	NO2 + NO3 ⇒ N2O5
IN-22	kt_{N2O5}	N2O5 ⇒ NO2 + NO3
IN-23	kt_{NO2+OH}	NO2 + OH + M ⇒ HNO3
IN-24	kt_{OH+NO}	OH + NO ⇒ HONO
Sulphate (inc. in-cloud) formation		
cl-OH	(b)	OH + SO2 ⇒ HO2 + SO4
cl-1	(b)	SO2 + H2O2 ⇒ SO4
cl-2	(b)	SO2 + O3 ⇒ SO4
cl-3	(b)	SO2 + Fe ⇒ SO4

Table S11: cont.

N	Rate coefficient	Reaction
Methane chemistry		
MA-1	$1.85 \times 10^{-20} \times T^{2.8} \ldots \ldots \times \exp(-987/T)$	OH + CH4 ⇒ CH3O2
MA-2	1.44×10^{-13}+ 3.43×10^{-33} M	OH + CO ⇒ HO2
MA-3	$2.3 \times 10^{-12} \exp(360/T)$	CH3O2 + NO ⇒ HCHO + HO2 + NO2
MA-4	$7.4 \times 10^{-13} \exp(-520/T)$	CH3O2 + CH3O2 ⇒ 2. HCHO + 2. HO2
MA-5	$1.03 \times 10^{-13} \exp(365/T)$ - $7.4 \times 10^{-13} \exp(-520/T)$	CH3O2 + CH3O2 ⇒ CH3OH + HCHO
MA-6	$6.38 \times 10^{-18} \exp(144/T) \times T^2$	OH + CH3OH ⇒ HO2 + HCHO + H2O
MA-7	$3.8 \times 10^{-13} \exp(780/T)$	HO2 + CH3O2 ⇒ 0.9 CH3O2H + 0.1 HCHO
MA-8	$5.3 \times 10^{-12} \exp(190/T)$	CH3O2H + OH ⇒ 0.4 HCHO + 0.4 OH + 0.6 CH3O2 + 0.6 H2O
Ethane and ethanol chemistry		
EA-1	$1.25 \times 10^{-17} \times T^2 \ldots \ldots \times \exp(615/T)$	OH + HCHO ⇒ CO + HO2 + H2O
EA-2	$2.0 \times 10^{-12} \exp(-2440/T)$	NO3 + HCHO ⇒ HNO3 + CO + HO2
EA-3	$6.9 \times 10^{-12} \exp(-1000/T)$	OH + C2H6 ⇒ C2H5O2 + H2O
EA-4	$2.55 \times 10^{-12} \exp(380/T)$	C2H5O2 + NO ⇒ HO2 + CH3CHO + NO2
EA-5	$3.8 \times 10^{-13} \exp(900/T)$	C2H5O2 + HO2 ⇒ C2H5OOH
EA-6	8.01×10^{-12}	C2H5OOH + OH ⇒ CH3CHO + OH
EA-7	$k_{OH+ROOH}$	C2H5OOH + OH ⇒ C2H5O2
EA-8	$4.4 \times 10^{-12} \exp(365/T)$	OH + CH3CHO ⇒ 0.95 CH3COO2 + 0.05 CH3O2 + 0.05 CO
EA-9	kt_{panf}	CH3COO2 + NO2 + M ⇒ PAN
EA-10	kt_{panb}	PAN + M ⇒ CH3COO2 + NO2
EA-11	$7.5 \times 10^{-12} \exp(290/T)$	CH3COO2 + NO ⇒ NO2 + CH3O2 + CO2
EA-12	$2.0 \times 10^{-12} \exp(500/T)$	CH3O2 + CH3COO2 ⇒ 0.9 HO2 + HCHO + 0.9 CH3O2 + 0.1 CH3COOH
EA-13	$2.9 \times 10^{-12} \exp(500/T)$	CH3COO2 + CH3COO2 ⇒ CH3O2 + CH3O2
EA-14	$5.2 \times 10^{-13} \exp(980/T)$	CH3COO2 + HO2 ⇒ 0.41 CH3COO2H + 0.15 O3 + 0.44 OH + 0.44 CH3O2 + 0.15 CH3COOH
EA-15	$1.9 \times 10^{-12} \exp(190/T)$	CH3COO2H + OH ⇒ CH3COO2
EA-16	$6.7 \times 10^{-18} \exp(511/T) \times T^2$	OH + C2H5OH ⇒ CH3CHO + HO2

Table S11: cont.

N	Rate coefficient	Reaction
n-butane chemistry		
NB-1	$2.03 \times 10^{-17} \exp(78/T)\ T^2$	OH + NC4H10 ⇒ SECC4H9O2
NB-2	k_{NO+RO2}	NO + SECC4H9O2 ⇒ NO2 + 0.65 HO2 + 0.65 MEK + 0.35 CH3CHO + 0.35 C2H5O2
NB-3	0.625×$k_{HO2+RO2}$	SECC4H9O2 + HO2 ⇒ BURO2H
NB-4	$2.53 \times 10^{-18} \exp(503/T)\ T^2$	OH + MEK ⇒ MEKO2
NB-5	k_{NO+RO2}	MEKO2 + NO ⇒ NO2 + CH3COO2 + CH3CHO
NB-6	0.625×$k_{HO2+RO2}$	MEKO2 + HO2 ⇒ MEKO2H
NB-7	$1.9 \times 10^{-12} \exp(190/T)$	MEKO2H + OH ⇒ MEKO2
NB-8	$k_{OH+ROOH}$	BURO2H + OH ⇒ SECC4H9O2
NB-9	2.15×10^{-11}	BURO2H + OH ⇒ OH + MEK
Ethene chemistry		
EE-1	$kt_{OH+C2H4}$	C2H4 + OH + M ⇒ ETRO2
EE-2	k_{NO+RO2}	ETRO2 + NO ⇒ NO2 + 2. HCHO + HO2
EE-3	1.2×10^{-11}	ETRO2 + HO2 ⇒ ETRO2H
EE-4	1.38×10^{-11}	ETRO2H + OH ⇒ CH3CHO + OH
EE-5	$k_{OH+ROOH}$	ETRO2H + OH ⇒ ETRO2
EE-6	$9.1 \times 10^{-15} \exp(-2580/T)$	C2H4 + O3 ⇒ 1.14 HCHO + 0.63 CO + 0.13 HO2 + 0.13 OH + 0.14 H2O2 + 0.23 HCOOH
Propene chemistry		
PE-1	$5.5 \times 10^{-15} \exp(-1880/T)$	O3 + C3H6 ⇒ 0.545 HCHO + 0.545 CH3CHO + 0.56 CO + 0.36 OH + 0.28 HO2 + 0.09 H2O2 + 0.1 CH4 + 0.28 CH3O2 + 0.075 HCOOH + 0.075 CH3COOH
PE-2	$kt_{OH+C3H6}$	OH + C3H6 + M ⇒ PRRO2
PE-3	k_{NO+RO2}	NO + PRRO2 ⇒ NO2 + CH3CHO + HCHO + HO2
PE-4	0.52×$k_{HO2+RO2}$	PRRO2 + HO2 ⇒ PRRO2H
PE-5	2.44×10^{-11}	PRRO2H + OH ⇒ ACETOL + OH
PE-6	$k_{OH+ROOH}$	PRRO2H + OH ⇒ PRRO2

Table S11: cont.

N	Rate coefficient	Reaction
o-xylene chemistry		
OX-1	1.36×10^{-11}	OXYL + OH ⇒ OXYO2
OX-2	k_{NO+RO2}	OXYO2 + NO ⇒ NO2 + MGLYOX + MAL + HO2
OX-3	0.859×$k_{HO2+RO2}$	OXYO2 + HO2 ⇒ OXYO2H
OX-4	4.2×10^{-11}	OXYO2H + OH ⇒ OXYO2
OX-5	5.58×10^{-11}	MAL + OH ⇒ MALO2
OX-6	k_{NO+RO2}	MALO2 + NO ⇒ NO2 + HO2 + MGLYOX + GLYOX
OX-7	0.706×$k_{HO2+RO2}$	MALO2 + HO2 ⇒ MALO2H
OX-8	$1.9 \times 10^{-12} \exp(190/T)$	MALO2H + OH ⇒ MALO2
OX-9	$6.6 \times 10^{-18} \exp(820/T) \times T^2$	OH + GLYOX ⇒ HO2 + 2 CO
Isoprene chemistry		
IS-1	$1.03 \times 10^{-14} \exp(-1995/T)$	C5H8 + O3 ⇒ 0.67 MACR + 0.26 MVK + 0.3 OP + 0.55 OH + 0.07 C3H6 + 0.8 HCHO + 0.06 HO2 + 0.05 CO
IS-2	$2.7 \times 10^{-11} \exp(390/T)$	C5H8 + OH ⇒ ISRO2
IS-3	k_{NO+RO2}	ISRO2 + NO ⇒ 0.32 MACR + 0.42 MVK + 0.74 HCHO + 0.14 ISNI + 0.12 ISRO2 + 0.78 HO2 + 0.86 NO2
IS-4	0.706×$k_{HO2+RO2}$	ISRO2 + HO2 ⇒ ISRO2H
IS-5	$2.6 \times 10^{-12} \exp(610/T)$	MVK + OH ⇒ MVKO2
IS-6	k_{NO+RO2}	MVKO2 + NO ⇒ 0.684 CH3CHO + 0.684 CH3COO2 + 0.266 MGLYOX + 0.266 HCHO + 0.05 ISNI + 0.95 NO2 + 0.95 HO2
IS-7	7.5×10^{-11}	ISRO2H + OH ⇒ OH + ISRO2
IS-8	$1.36 \times 10^{-15} \exp(-2112/T)$	MACR + O3 ⇒ 0.59 MGLYOX + 0.41 HO2 + 0.82 CO + 0.82 OH + 0.534 HCHO + 0.124 H2O2 + 0.41 CH3COO2 +0.056 HCOOH
IS-9	$8.0 \times 10^{-12} \exp(380/T)$	MACR + OH ⇒ 0.5 MACRO2 + 0.5 MACO3
IS-10	kt_{panf}	MACO3 + NO2 ⇒ MPAN
IS-11	kt_{panb}	MPAN ⇒ MACO3 + NO2
IS-12	$7.6 \times 10^{-12} \exp(180/T)$	MACRO2 + NO ⇒ 0.95 HO2 + 0.95 CO + 0.95 ACETOL + 0.05 ISNI + 0.95 NO2
IS-13	2.5×10^{-12}	MACRO2 + NO3 ⇒ NO2 + ACETOL + HCHO + HO2
IS-14	0.625×$k_{HO2+RO2}$	MACRO2 + HO2 ⇒ MACROOH +O2
IS-15	2.82×10^{-11}	MACROOH + OH ⇒ MACRO2
IS-16	$1.6 \times 10^{-12} \exp(305/T)$	ACETOL + OH ⇒ MGLYOX + HO2
IS-17	$8.7 \times 10^{-12} \exp(290/T)$	MACO3 + NO ⇒ CH3COO2 + HCHO + NO2

Table S11: cont.

N	Rate coefficient	Reaction
Isoprene cont.		
IS-18	$8.5 \times 10^{-16} \exp(-1520/T)$	MVK + O3 ⇒ 0.82 MGLYOX + 0.8 HCHO + 0.2 OP + 0.05 CO + 0.06 HO2 + 0.04 CH3CHO + 0.08 OH
IS-19	5.96×10^{-11}	ISNI + OH ⇒ ISNIR
IS-20	k_{NO+RO2}	ISNIR + NO ⇒ 0.05 ISNI + 0.05 HO2 + 1.9 NO2 + 0.95 CH3CHO + 0.95 ACETOL
IS-21	$3.15 \times 10^{-12} \exp(-450/T)$	C5H8 + NO3 ⇒ ISONO3
IS-22	k_{NO+RO2}	ISONO3 + NO ⇒ 1.1 NO2 + 0.8 HO2 + 0.85 ISNI + 0.1 MACR + 0.15 HCHO + 0.05 MVK
IS-23	0.706×$k_{HO2+RO2}$	ISONO3 + HO2 ⇒ ISONO3H
IS-24	0.625×$k_{HO2+RO2}$	MVKO2 + HO2 ⇒ MVKO2H
IS-25	$4.3 \times 10^{-13} \exp(1040/T)$	MACO3 + HO2 ⇒ 0.71 MACO3H + 0.29 MACO2H + 0.29 O3
IS-26	1.87×10^{-11}	MACO3H + OH ⇒ MACO3
IS-27	1.51×10^{-11}	MACO2H + OH ⇒ CH3COO2 + HCHO
IS-28	0.706×$k_{HO2+RO2}$	ISNIR + HO2 ⇒ ISNIRH
IS-29	2.0×10^{-11}	ISONO3H + OH ⇒ ISONO3
IS-30	2.2×10^{-11}	MVKO2H + OH ⇒ MVKO2
IS-31	3.7×10^{-11}	ISNIRH + OH ⇒ ISNIR
IS-32	2.9×10^{-11}	MPAN + OH ⇒ ACETOL + CO + NO2
		Miscelleneous
MS-1	2.1E-6	RN222 ⇒ PB210
MS-2	1.0E-12×H2O	PB210 ⇒ aerosol sink
MS-3	1.0E-5	H2O2 ⇒ aerosol sink
MS-4	1.0E-5	CH3O2H ⇒ aerosol sink
MS-5	k_{ECage}	ECnew_f ⇒ ECage_f

Notes. T is temperature, M is third body; Reaction coefficients are in units of s^{-1} for unimolecular reactions, cm^3 $molecule^{-1}$ s^{-1} for bimolecular reactions, and cm^6 $molecule^{-2}$ s^{-2} for termolecular reactions. Reaction steps labelled as "Immediate" are given for clarity only. Rate-coefficients labelled with kt are given as Troe expressions in Table S12, and coefficients labelled with k are given in Table S13 (except (a), below). (a) k_{N2O5} discussed in Sect. 7.7, main article. (b) The 'cl' rates for sulphate formation involve cloud-water calculations and are discussed in Sect. 7.5–7.6, main article.

Table S12: Rate-constants for 3-body reactions using the Troe expression[(a)] The reaction rates are calculated as: $k = \frac{k_0 k_\infty}{k_0 + k_\infty} F$, with the broadening factor F calculated using the approximate expression: $\log_{10} F \cong \frac{\log_{10} F_c}{1+[\log_{10}(k_0/k_\infty)/N]^2}$ where $N = [0.75 - 1.27 \log_{10} F_c]$ The first column (Rate coeff.) refers to the notation in Table S11.

Rate coeff.	$k_0/[M]$	k_∞	F_c
kt_{NO+OP}	$1.0 \times 10^{-31}(300/T)^{1.6}$	$3.0 \times 10^{-11}(300/T)^{-0.3}$	0.85
$kt_{NO2+NO3}$	$3.6 \times 10^{-30}(300/T)^{4.1}$	$1.9 \times 10^{-12}(300/T)^{-0.2}$	0.35
kt_{N2O5}	$1.3 \times 10^{-3}(300/T)^{3.5} e^{(-11000/T)}$	$9.70 \times 10^{14}(300/T)^{-0.1}\ e^{(-11080/T)}$	0.35
kt_{NO2+OH}	$3.3e \times 10^{30}(300/T)^{3.0}$	4.1×10^{-11}	0.40
kt_{OH+NO}	$7.4 \times 10^{-31}(300/T)^{2.4}$	$3.3 \times 10^{-11}(300/T)^{0.3}$	$e^{(-T/1420)}$
$kt_{OH+C2H4}$	$8.6 \times 10^{-29}(300/T)^{3.1}$	$9.0 \times 10^{-12}(300/T)^{0.85}$	0.48
kt_{NO+OP}	$1.0 \times 10^{-31}(300/T)^{1.6}$	$3.0 \times 10^{-11}(300/T)^{-0.3}$	0.85
$kt_{OH+C3H6}$	$8.0 \times 10^{-27}(300/T)^{3.5}$	$3.0 \times 10^{-11} \exp(300/T)$	0.5
kt_{panf}	$2.7 \times 10^{-28}(300/T)^{7.1}$	$1.2 \times 10^{-11}(300/T)^{0.9}$	0.3
kt_{panb}	$4.9 \times 10^{-3}(300/T)^{-12100}$	$5.4 \times 10^{16} \exp(-13830/T)$	0.3

(a) For form of Troe expressions, see eg Atkinson et al. (2006)).

Table S13: Other rate coefficients

No.	rate	Comments
$k_{OH+HNO3}$	= $K_1 + (K_3[M])/(1.0 + (K_3[M])/K_4)$, where $K_1 = 2.4 \times 10^{-14} \exp(460/T)$ $K_2 = 6.5 \times 10^{-34} \exp(1335/T)$ $K_3 = 2.7 \times 10^{-17} \exp(2199/T)$	
$k_{HO2+HO2}$	= $F_{H2O} \times 2.2 \times 10^{-13} \exp(600/T)\ldots$ + $F_{H2O} \times 1.9 \times 10^{-33} \exp(980/T) \times M$,	where F_{H2O} = $1+1.4 \times 10^{-21} \exp(2200/T)[H2O]$
$k_{OH+ROOH}$	= $1.9 \times 10^{-12} \exp(190/T)$	
$k_{HO2+RO2}$	= $2.91 \times 10^{-13} \exp(1300/T)$	
k_{NO+RO2}	= $2.54 \times 10^{-12} \exp(360/T)$	
k_{aero}	=1.0×10^{-5} when RH>90%, else 5.0×10^{-6}	
k_{ECage} (day)	=3.3×10^{-6} for lowest 3 layers (<300m approx) =1.4×10^{-4} for upper layers (>300m approx)	Tsyro et al. (2007)
k_{ECage} (night)	=1.0×10^{-5} for lowest 3 layers (<300m approx)	

Table S14: Photolysis reactions. For some reactions, rates are taken from given surrogate species, scaled if necessary

N	Reaction
J-O3A	O3 ⇒ OP
J-O3B	O3 ⇒ OD
J-NO2	NO2 ⇒ OP + NO
J-H2O2	H2O2 ⇒ 2 OH
J-HNO3	HNO3 ⇒ NO2 + OH
J-HCHOA	HCHO ⇒ CO + 2 HO2
J-HCHOB	HCHO ⇒ CO + H2
J-CH3CHO	CH3CHO ⇒ CH3O2 + HO2 + CO
J-NO3	NO3 ⇒ NO2 + OP
J-CH3O2H	CH3O2H ⇒ HCHO + OH + HO2
J-GLYOX	GLYOX ⇒ 1.9 CO + 0.1 HCHO + 0.5 HO2
J-RCOHCO	MGLYOX ⇒ CH3COO2 + CO + HO2
J-CH3O2H	C2H5OOH ⇒ HO2 + CH3CHO + OH
J-CH3O2H	ETRO2H ⇒ HO2 + OH + 1.56 HCHO + 0.22 CH3CHO
J-CH3O2H	BURO2H ⇒ OH + 0.65 HO2 + 0.65 MEK + 0.35 CH3CHO + 0.35 C2H5O2
J-CH3O2H	PRRO2H ⇒ CH3CHO + HCHO + HO2
J-CH3O2H	MEKO2H ⇒ CH3CHO + CH3COO2 + OH
J-CH3COX	MEK ⇒ CH3COO2 + C2H5O2
J-CH3O2H	CH3COO2H ⇒ CH3O2 + OH
J-CH3O2H	OXYO2H ⇒ OH + MGLYOX + MAL + HO2
J-CH3O2H	MALO2H ⇒ OH + HO2 + MGLYOX + GLYOX
0.222 J-NO2	HONO ⇒ OH + NO

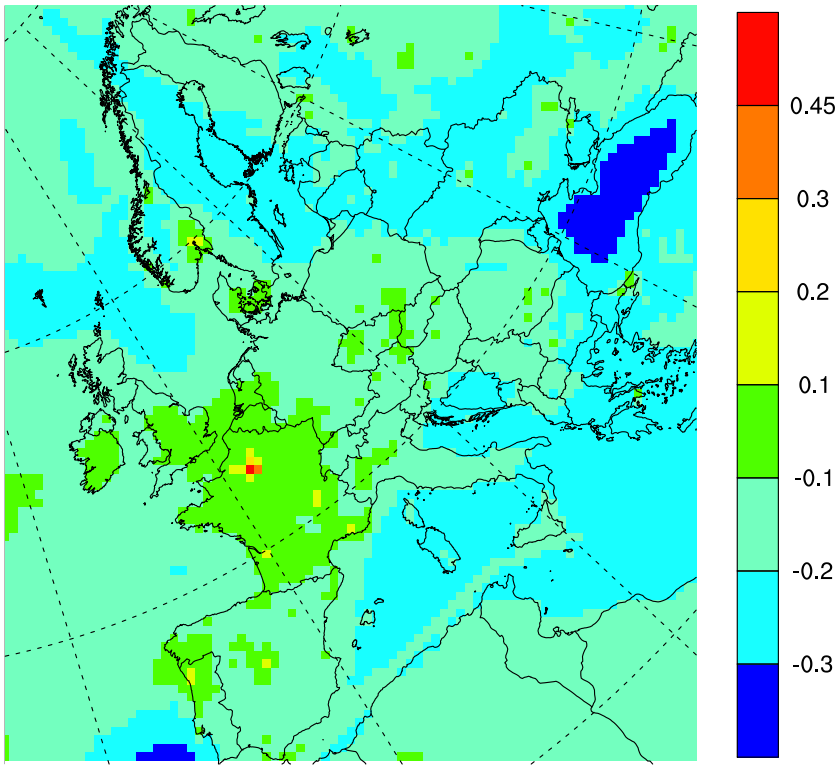

Figure S2: Relative difference in fine organic aerosol concentrations obtained using the NPAS scheme (with inert POA) to those obtained with the PAA scheme of Bergström et al. 2012, which has volatile POA emissions and atmospheric aging of the emitted semi- and intermediate volatility OC. Calculations for the year 2006. (Relative difference defined as: [NPAS-PAA]/PAA).

S6 Sensitivity test: POA

As discussed in Sects. 7.9 and 12, the 'standard' EMEP model, using our so-called NPAS version of the VBS methodology, assumes that primary organic aerosol (POA) emissions are inert, whereas the research versions of the model presented by Bergström et al. (2012) have allowed for the volatility of POA emissions and also introduced related emissions of semi- and intermediate-volatility gases. Fig. S2 shows the relative difference in modelled OA concentrations using the NPAS assumptions compared to a scheme (PAA, see Bergström et al. 2012) using these more complex VBS assumptions. The results are discussed in Sect. 12.

S7 Dry deposition, additional information

S7.1 Leaf area index calculations

Leaf area index (LAI, which is one-sided, projected) is calculated according to Table S15, making use of Table 3.

Table S15: Calculation of LAI as a function of daynumber d_n, start and end days of growing season (d_{SGS}, d_{EGS}), and other parameters as given in Table 3. See also Fig. 4.

Time of year	LAI
$d_n \le d_{SGS}$ or $d_n \ge d_{EGS}$	LAI_{min}
$d_{SGS} < d_n \le d_{SGS} + L_S$	$\text{LAI}_{\text{min}} + (\text{LAI}_{\text{max}} - \text{LAI}_{\text{min}})(d_n - d_{SGS})/L_S$
$d_{SGS} + L_S < d_n \le d_{EGS} - L_E$	LAI_{max}
$d_{EGS} - L_E < d_n < d_{EGS}$	$\text{LAI}_{\text{min}} + (\text{LAI}_{\text{max}} - \text{LAI}_{\text{min}})(d_{EGS} - d_n)/L_E$

S7.2 Stomatal conductance calculations

As noted in Sect. 8.5, the calculation of stomatal conductance acording to the DO_3SE algorithm requires the calculation of factors accounting for time of year (leaf phenology factor, f_{phen}), the minimum observed stomatal conductance (f_{min}), light (PAR, with factor f_{light}), temperature (f_T), vapour-pressure deficit (D, factor f_{D}), and soil-water (SW, factor f_{SW}). Such functions and their parameters have been presented widely in the literature, and in LRTAP (2009). However, the values and equations have been modified over the years. Here we present the equations and parameter values used in the current (rv4) EMEP model. These are loosely based upon those presented in LRTAP (2009), but (especially in the case of f_{phen}) simplified somewhat to match the limitations inherent in large-scale modelling. As an important example, we have shown previously that even such basic parameters as the start of the growing season are difficult to capture with European-wide models (Tuovinen et al., 2009).

Table S16 lists g_{max} values (given at normal temperature and pressure, in mmole $O_3\,m^{-2}$ (PLA) s^{-1}, denoted g^m_{max}) along with values of other parameters needed for the conductance modelling. For pressure P and temperature T, g_{max} in $m\,s^{-1}$ units is given by:

$$g_{max} = g^m_{max} R\, T/P \tag{12}$$

R is here the gas-constant (8.314 $J\,mole^{-1}\,K^{-1}$). At normal temperature and pressure, $g_{max} \approx g^m_{max}/41000$. The canopy average stomatal conductance, g_{sto}, is calculated as:

$$g_{sto} = g_{max}\ f_{phen}\ f_{light}\ \max(f_{min}, f_T\ f_D\ f_{SW}) \tag{13}$$

Table S16 gives the landcover species parameters associated with f_{phen}, f_{light}, f_T and f_{D}. f_{phen} is calculated according to Table S17, and is illustrated for two land-cover types in Fig. S3. The summertime dip in f_{phen} for the Mediterranean species is intended to reflect the well-documented effects of drought-stress on vegetation in this area, although it is an open question

if this procedure is double-counted in the f_{SW} function (see Alonso et al., 2008, for contrasting examples).

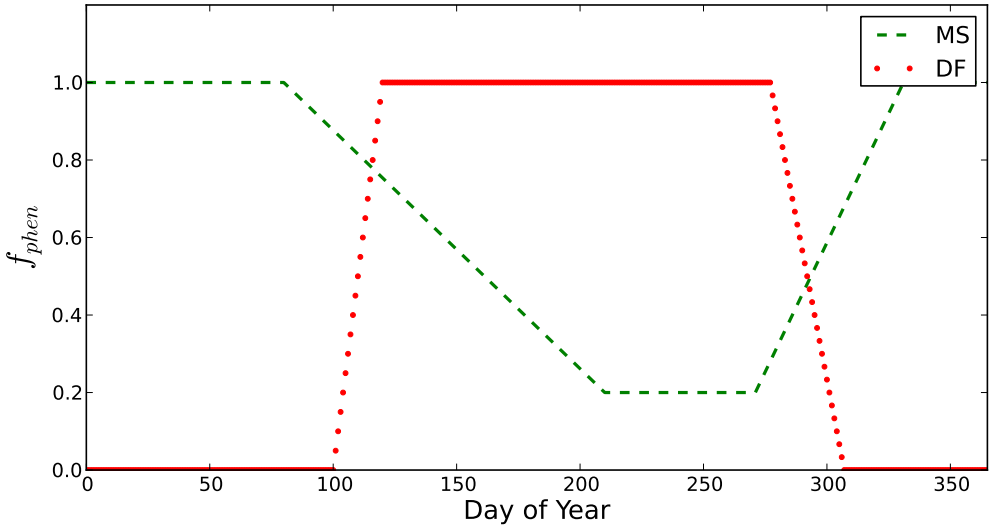

Figure S3: Illustration of f_{phen} function for two contrasting land-cover classes, DF (temperature/boreal deciduous, here at 50° N) and (MS) Mediterranean scrub.

Table S16: Land-cover specific parameters for stomatal conductance (DO_3SE) calculations

Code	g^m_{max}	f_{min}	f_{phen} factors								f_{light}	f_T			f_D		
			ϕ_a	ϕ_b	ϕ_c	ϕ_d	ϕ_e	ϕ_f	ϕ_{A_S}	ϕ_{A_E}	α	Tmin	Topt	Tmax	Dmax	Dmin	ΣDCrit.
	†						days	days	days	days		°C	°C	°C	kPa	kPa	kPa
CF	140	0.1	0.8	0.8	0.8	0.8	1	1	0	0	0.006	0	18	36	0.5	3	
DF	150	0.1	0	0	1	0	20	30	0	0	0.006	0	20	35	1	3.25	
NF	200	0.1	1	1	0.2	1	130	60	80	35	0.013	8	25	38	1	3.2	
BF	200	0.02	1	1	0.3	1	130	60	80	35	0.009	1	23	39	2.2	4	
TC	300	0.01	0.1	0.1	1	0.1	0	45	0	0	0.0105	12	26	40	1.2	3.2	8
MC	300	0.019	0.1	0.1	1	0.1	0	45	0	0	0.0048	0	25	51	1	2.5	
RC	360	0.02	0.2	0.2	1	0.2	20	45	0	0	0.0023	8	24	50	0.31	2.7	10
SNL	60	0.01	1	1	1	1	1	1	0	0	0.009	1	18	36	1.3	3	
GR	270	0.01	1	1	1	1	0	0	0	0	0.009	12	26	40	1.3	3	
MS	200	0.01	1	1	0.2	1	130	60	80	35	0.012	4	20	37	1.3	3.2	
IAM_CR	500	0.01	0.1	0.1	1	0.1	0	45	0	0	0.0105	12	26	40	1.2	3.2	8
IAM_DF	150	0.1	0	0	1	0	15	20	0	0	0.006	0	21	35	1	3.25	
IAM_MF	175	0.02	1	1	0.3	1	130	60	80	35	0.009	2	23	38	2.2	4	

Notes: † Units of g^m_{max} are mmole O_3 m^{-2} (PLA) s^{-1}

Table S17: Definition of phenology function, f_{phen} as a function of daynumber d_n, start and end of growing season (d_{SGS}, d_{EGS}), and other parameters as given in Table S16

Time of year	f_{phen}
$d_n \leq d_{SGS}$ or $d_n > d_{EGS}$	0
$d_{SGS} < d_n \leq A_{start}$	ϕ_a
$A_{start} < d_n \leq A_{start} + \phi_e$	$\phi_b + (\phi_c - \phi_b)(d_n - A_{start})/\phi_e$
$A_{start} + \phi_e < d_n \leq A_{end} - \phi_f$	ϕ_c
$A_{end} - \phi_f < d_n \leq A_{end}$	$\phi_d + (\phi_c - \phi_d)(A_{end} - d_n)/\phi_f$
$A_{end} < d_n \leq d_{EGS}$	ϕ_d

Notes: A_{start} calculated from $d_{SGS}+\phi_{A_S}$, A_{end} from $d_{EGS}-\phi_{A_E}$, c.f. Table S16.

Calculation of $f_{\rm light}$ makes use of the photosyntheric active radiation components, $I_{\rm PAR}^{\rm sun}$ and $I_{\rm PAR}^{\rm shade}$, as presented in Sect. 4. We calculate the effects for sun and shade leaves with:

$$f_{sun} = \quad 1 - e^{-\alpha I_{\rm PAR}^{\rm sun}} \tag{14}$$

$$f_{shade} = \quad 1 - e^{-\alpha I_{\rm PAR}^{\rm shade}} \tag{15}$$

where α values are land-cover specific and given in Table S16 Given the fraction of leaves in sun (f_{LAI}^{sun} = LAI$_{sun}$/LAI, Sect. 4), the canopy average $f_{\rm light}$ is calculated as:

$$f_{light} = f_{LAI}^{sun}\ f_{sun} + (1 - f_{LAI}^{sun})\ f_{shade} \tag{16}$$

Calculation of f_T uses the 2m air temperature T_2, together with parameters from Table S16:

$$f_T = \frac{T_2 - T_{\rm min}}{T_{\rm opt} - T_{\rm min}} \left(\frac{T_{\rm max} - T_2}{T_{\rm max} - T_{\rm opt}} \right)^{\beta} \tag{17}$$

where β is given by $(T_{\rm max} - T_{\rm opt})/(T_{\rm opt} - T_{\rm min})$. f_T is constrained with a minumum value of 0.01 (all temperatures here are in $^\circ$ C). The effects of humidity are accounted for with $f_{\rm D}$, with the basic calculation given by:

$$f_D = f_{min} + (1 - f_{min}) \frac{D_{min} - D}{D_{min} - D_{max}} \tag{18}$$

f_D is further constrained to lie bewteen f_{min} and 1.0.

For a few landcover categories (see Table S16), $\Sigma D_{\rm Crit.}$ values are specified. For these land-covers, we also calculate ΣD (h), the hourly time-integral all vapour pressure deficits from sun-rise until the curret hour, h. ΣD accumulates over the day, and when ΣD (h) exceeds $\Sigma D_{\rm Crit.}$, then we enforce:

$$g_{\rm sto}(h) \leq g_{\rm sto}(h-1) \tag{19}$$

This procedure is mainly desiged to prevent afternoon $g_{\rm sto}$ increasing after a period of morning water stress, as suggested by Uddling et al. (2004) and LRTAP (2009).

As noted in Sect. 3.3, soil water (SW) is very difficult to model accurately in large-scale models, and the soil moisture index, S_{MI} is used instead. The equation used for $f_{\rm SW}$ is given in Sect.8.5 (Eq. 58) of the main text.

S7.3 Properties of gases for dry deposition

Table S18: Properties of gases for dry deposition calculations. Diffusivity ratio for a gas i, $D_r = D_{H2O}/D_i$, Solubility index H_* (based upon Effective Henry's coefficient), and Reactivity index f_o. Based upon Wesely et al. (1985).

Gas	D_r	H_*	f_o
SO2	1.9	1.0×10^{5}	0.0
O3	1.6	1.0×10^{-2}	1.0
NO2	1.6	1.0×10^{-2}	0.1
HNO3	1.9	1.0×10^{14}	0.0
H2O2	1.4	1.0×10^{5}	1.0
HCHO	1.3	6.0×10^{3}	0.0
ALD$^{(a)}$	1.6	15	0.0
OP$^{(b)}$	1.6	2.4×10^{2}	0.1
NH3$^{(c)}$	1.0	1.0×10^{5}	0.0
PAN	2.6	3.6	0.1

Notes: (a) Used for all aldehydes except HCHO; (b) OP=Wesely "Methyl hydroperoxide" - used for all hyroperoxides (c) H^* increased compared to Wesely value, reflecting European pH conditions.

Table S19: Base-values of ground-surface resistance for sulphur dioxide ($\hat{R}_{gs}^{SO_2}$) and ozone ($\hat{R}_{gs}^{O_3}$). Units: s m^{-1}.

Landuse	$\hat{R}_{gs}^{SO_2}$	$\hat{R}_{gs}^{O_3}$
Forests, Mediterranean scrub	-	200
Crops	-	200
Moorland	-	400
Grasslands	-	1000
Wetlands	50	400
Tundra	500	400
Desert	1000	2000
Water	1	2000
Ice+snow	1000	2000
Urban	400	400

Notes: '-' - denotes other formulation, using resistances calculated as given in Sect. 8.7.

S8 Wet deposition, additional information

Table S20: Wet scavenging ratios and collection efficiencies used in the EMEP MSC-W model.

Components$^{(a)}$	W$_{in}$ ($\times 10^6$)	W$_{sub}$ ($\times 10^6$)	$\bar{E}$	Comment
SO_2	0.3	0.15	-	
HNO_3, HONO, NH_3, H_2O_2	1.4	0.5	-	
HCHO	0.1	0.03	-	
ROOH	0.05	0.015	-	
PMf	1.0	-	0.02	Generic fine patricles, includes SO_4^{2-}, NH_4^-, fine-NO_3^-, ECage_f, OA$^{(b)}$, fine-dust
PMecf	0.2	-	0.02	Fresh (hydrophobic) ECnew_f
PMssf	1.6	-	0.02	Fine sea-salt
PMssc	1.6	-	0.4	Coarse sea-salt
PMc	1.0	-	0.4	Other coarse patricles, includes coarse: NO_3^-, PPM, dust

(a) ROOH, and PM- type components are generic labels, see also Table S5 for particles associated with these rates; (b) For semi-volatile compounds associated with organic aerosol (OA), only the particle fraction is scavenged.

S8.1 Initial and boundary conditions, additional information

Table S21: Parameters used to set prescribed boundary conditions

	χ_{mean} ppb	d_{max} days	$\Delta\chi$ ppb	H_z km	χ^v_{min} ppb	χ^h_{min} ppb
SO2	0.15	15	0.05	∞	0.15	0.03
SO4	0.15	180	0.00	1.6	0.05	0.03
NO	0.1	15	0.03	4.0	0.03	0.02
NO2	0.1	15	0.03	4.0	0.05	0.04
PAN	0.20	120	0.15	∞	0.20	0.1
CO	125.0	75	35.0	25.0	70.0	30.0
HNO_3	0.07	180	0.03	∞	0.025	0.03
nitrate$^{(a)}$	0.07	15	0.03	1.6	0.025	0.02
NH_4^+	0.15	180	0.0	1.6	0.5	0.03
C2H6	2.0	75	1.0	10.0	0.05	0.05
C4H10	2.0	45	1.0	6.0	0.05	0.05
HCHO	0.7	180	0.3	6.0	0.05	0.05
CH3CHO	0.3	180	0.05	6.0	0.005	0.005
Seasalt fine	0.5	15	0.3	1.6	0.01	0.01
Seasalt coarse	3.0	15	1.0	1.6	0.01	0.01

Notes: See text for definition of terms. (a) same values used for both coarse and fine nitrate. Concentrations and other parameters estimated largely from Warneck (1988); Derwent et al. (1998); Ehhalt et al. (1991); Emmons et al. (2000); Isaksen and Hov (1987); Lewis et al. (2005); Millet et al. (2010); Penkett et al. (1993); Singh et al. (2004); Solberg et al. (1996, 2001) and University of Oslo CTM2 model (Sundet, 1997).

Table S22: Latitude factors applied to prescribed boundary and initial conditions.

Component	Latitude (° N)								
	30	35	40	45	50	55	60	65	70-90
SO2^a	0.05	0.15	0.3	0.8	1.0	0.6	0.2	0.12	0.05
HNO3^b	1.00	1.00	1.00	0.85	0.7	0.55	0.4	0.3	0.2
PAN	0.15	0.33	0.5	0.8	1.0	0.75	0.5	0.3	0.1
CO	0.6	0.7	0.8	0.9	1.0	1.0	0.95	0.85	0.8

Notes: (a) Applied also for SO_4, NO, NO_2; (b) Applied also for HCHO, CH_3CHO; See Simpson (1992) for sources of data

Table S23: Assumed trends for boundary concentrations

Species	Trend , pre-1990 %/year	Trend , post-1990 %/year	Notes
O3	1	(a)	(b)
CO	0.85	0	(c)
VOC	0.85	0	(d)
CH4	0.91	0.2	(e)

Notes: (a) Mace-head correction applied on yearly basis to climatological values from 1990-current year, see section 10-1. (b) pre-1990 from Janach (1989); Low et al. (1990); Volz and Kley (1988); Bojkov (1986); Logan (1994) (c) Trend for CO of 0.85%/yr from Zander et al. (1989b); (d) Trend for ethane of 0.85%/yr from Ehhalt et al. (1991). Same trends assumed for n-butane and ethene. (e) Pre-1990 values from Zander et al. (1989a) for 1975-1990. Post-1990 values valid for 1990-2000, derived from Mace-Head observations.

References

Aas, W., Tsyro, S., Bieber, E., Bergström, R., Ceburnis, D., Ellermann, T., Fagerli, H., Frölich, M., Gehrig, R., Makkonen, U., Nemitz, E., Otjes, R., Perez, N., Perrino, C., Prévôt, A. S. H., Putaud, J.-P., Simpson, D., Spindler, G., Vana, M., and Yttri, K. E.: Lessons learnt from the first EMEP intensive measurement periods, Atmospheric Chemistry and Physics Discussions, 12, 3731–3780, doi:10.5194/acpd-12-3731-2012, URL http://www.atmos-chem-phys-discuss.net/12/3731/2012/, 2012.

Alonso, R., Elvira, S., Sanz, M. J., Gerosa, G., Emberson, L. D., Bermejo, V., and Gimeno, B. S.: Sensitivity analysis of a parameterization of the stomatal component of the DO3SE model for Quercus ilex to estimate ozone fluxes, Environ. Poll., 155, 473–480, doi:10.1016/j.envpol.2008.01.032, 2008.

Atkinson, R., Baulch, D. L., Cox, R. A., Crowley, J. N., Hampson, R. F., Hynes, R. G., Jenkin, M. E., Rossi, M. J., Troe, J., and Subcommittee, I.: Evaluated kinetic and photochemical data for atmospheric chemistry: Volume II – gas phase reactions of organic species, Atmos. Chem. Physics, 6, 3625–4055, URL http://www.atmos-chem-phys.net/6/3625/2006/, 2006.

Bergström, R., Denier van der Gon, H., Prevot, A., Yttri, K., and Simpson, D.: Modelling of organic aerosols over Europe (2002-2007) using a volatility basis set (VBS) framework with application of different assumptions regarding the formation of secondary organic aerosol, Atmos. Chem. Physics, 12, 5425–5485, 2012.

Bojkov, R.: Surface ozone concentrations during the second half of the nineteenth century, J. Clim. Appl. Met., 25, 343–352, 1986.

Derwent, R., Simmonds, P., Seuring, S., and Dimmer, C.: Observations and interpretation of the seasonal cycles in the surface concentrations of ozone and carbon monoxide at Mace Head, Ireland from 1990 to 1994, Atmos. Environ., 32, 145–157, 1998.

Ehhalt, D.H.and Schmidt, U., Zander, R., Demoulin, P., and Rinsland, C.: Seasonal cycle and secular trend of the total and tropospheric column abundance of ethane above the Jungfraujoch, J. Geophys. Res., 96, 4985–4994, d3, 1991.

Emmons, L. K., Hauglustaine, D. A., Mller, J.-F., Carroll, M. A., Brasseur, G. P., Brunner, D., Staehelin, J., Thouret, V., and Marenco, A.: Data composites of airborne observations of tropospheric ozone and its precursors, J. Geophys. Res., 105, 20 497–20 538, URL http://dx.doi.org/10.1029/2000JD900232, 2000.

Gong, S., Barrie, L., and Blanchet, J.: Modeling sea-salt aerosols in the atmosphere .1. Model development, J. Geophys. Res., 102, 3805–3818, doi:{10.1029/96JD02953}, 1997.

Hayman, G., Bergström, R., Jenkin, M., and Simpson, D.: Modelling Photochemical Oxidants in Europe: benchmarking seven chemical mechanisms, In preparation, 2012.

Isaksen, I. and Hov, Ø.: Calculation of trends in the tropospheric concentration of O_3, OH, CO, CH_4 and NO_x, Tellus, 39B, 271–285, 1987.

Janach, W.: Surface ozone: trend details, seasonal variations, and interpretation, J. Geophys. Res., 94, 18 289–18 295, d15, 1989.

Jonson, J. E., Travnikov, O., Gauss, M., Gusev, A., Iyin, I., Valiyaveetil, S., Valdebenito, A., Wind, P., Sokovykh, V., Shatalov, V., Lin, C.-J., Dastoor, A., MacLeod, M., and Hollander, A.: Development of the EMEP global modelling framework: Progress report, EMEP/MSC-W Technical Report 1/2010, The Norwegian Meteorological Institute, Oslo, Norway, 2010.

Lewis, A. C., Hopkins, J. R., Carpenter, L. J., Stanton, J., Read, K. A., and Pilling, M. J.: Sources and sinks of acetone, methanol, and acetaldehyde in North Atlantic marine air, Atmos. Chem. Physics, 5, 1963–1974, URL http://www.atmos-chem-phys.net/5/1963/2005/, 2005.

Logan, J.: Trends in the vertical distribution of ozone: An analysis of ozonesonde data, J. Geophys. Res., 99, 25 553–25 585, 1994.

Low, P., Davies, T., Kelly, P., and Farmer, G.: Trends in surface ozone at Hohenpeissenberg and Arkona, J. Geophys. Res., 95, 22 441–22 453, d13, 1990.

LRTAP: Mapping critical levels for vegetation, in: Manual on Methodologies and Criteria for Mapping Critical Loads and Levels and Air Pollution Effects, Risks and Trends. Revision of 2009, edited by Mills, G., UNECE Convention on Long-range Transboundary Air Pollution. International Cooperative Programme on Effects of Air Pollution on Natural Vegetation and Crops, updated version available at www.icpmapping.com/, 2009.

Mårtensson, E., Nilsson, E., de Leeuw, G., Cohen, L., and Hansson, H.-C.: Laboratory simulations and parameterisation of the primary marine aerosol production, J. Geophys. Res., 108, 4297, doi:10.1029/2002JD002263, d9, 2003.

Millet, D. B., Guenther, A., Siegel, D. A., Nelson, N. B., Singh, H. B., de Gouw, J. A., Warneke, C., Williams, J., Eerdekens, G., Sinha, V., Karl, T., Flocke, F., Apel, E., Riemer, D. D., Palmer, P. I., and Barkley, M.: Global atmospheric budget of acetaldehyde: 3-D model analysis and constraints from in-situ and satellite observations, Atmos. Chem. Physics, 10, 3405–3425, 2010.

Monahan, E., Spiel, D., and Davidson, K.: A model of marine aerosol generation via white caps and wave disruption, in: Oceanic whitecaps, edited by Monahan, E. and MacNiochaill", G., pp. 167–193, Dordrecht: Reidel, The Netherlands, 1986.

Passant, N.: Speciation of UK emissions of non-methane volatile organic compounds, Report ENV-0545 ENV-0545, AEA Technology, Culham, Abingdon, United Kingdom, 2002.

Penkett, S., Blake, N., Lightman, P., Marsh, A., Anwyl, P., and Butcher, G.: The seasonal variation of nonmethane hydrocarbons in the free troposphere over the North Atlantic ocean: possible evidence for extensive reaction of hydrocarbons with the nitrate radical, J. Geophys. Res., 98, 2865–2885, 1993.

Simpson, D.: Long period modelling of photochemical oxidants in Europe. Calculations for July 1985, Atmos. Environ., 26A, 1609–1634, 1992.

Simpson, D., Fagerli, H., Jonson, J., Tsyro, S., Wind, P., and Tuovinen, J.-P.: The EMEP Unified Eulerian Model. Model Description, EMEP MSC-W Report 1/2003, The Norwegian Meteorological Institute, Oslo, Norway, 2003.

Singh, H. B., Salas, L. J., Chatfield, R. B., Czech, E., Fried, A., Walega, J., Evans, M. J., Field, B. D., Jacob, D. J., Blake, D., Heikes, B., Talbot, R., Sachse, G., Crawford, J. H., Avery, M. A., Sandholm, S., and Fuelberg, H.: Analysis of the atmospheric distribution, sources, and sinks of oxygenated volatile organic chemicals based on measurements over the Pacific during TRACE-P, J. Geophys. Res., 109, D15S07, doi:10.1029/2003JD003883, 2004.

Skålin, R., Lie, I., and Berge, E.: A parallel algorithm for simulation of long range transport of air pollution, in: High performance computing in the geosciences, edited by Dimet, F.-X. L., pp. 175–185, Kluwer Academic Publishers, 1995.

Solberg, S., Dye, C., Schmidbauer, N., Herzog, A., and Gehrig, R.: Carbonyls and nonmethane hydrocarbons at rural European sites from the Mediterranean to the Arctic, J. Atmos. Chem., 25, 33–66, 1996.

Solberg, S., Dye, C., Walker, S., and Simpson, D.: Long-term measurements and model calculations of formaldehyde at rural European monitoring sites, Atmos. Environ., 35, 195–207, 2001.

Sundet, J.: Model studies with a 3-d global CTM using ECMWF data, Ph.D. thesis, Department of Geophysics, University of Oslo, Norway, 1997.

Travnikov, O., Jonson, J. E., Andersen, A. S., Gauss, M., Gusev, A., Rozovskaya, O., Simpson, D., Sokovyh, V., Valiyaveetil, S., and Wind, P.: Development of the EMEP global modelling framework: Progress report, EMEP/MSC-E Technical Report 7/2009, 2009.

Tsyro, S., Simpson, D., Tarrasón, L., Kupiainen, K., Klimont, Z., Yttri, K., and Pio, C.: Modelling of black carbon over Europe, J. Geophys. Res., 112, D23S19, doi:10.1029/2006JD008164, 2007.

Tsyro, S., Aas, W., Soares, J., Sofiev, M., Berge, H., and Spindler, G.: Modelling of sea salt concentrations over Europe: key uncertainties and comparison with observations, Atmos. Chem. Physics, 11, 10 367–10 388, doi: 10.5194/acp-11-10367-2011, URL http://www.atmos-chem-phys.net/11/10367/2011/, 2011.

Tuovinen, J.-P., Emberson, L., and Simpson, D.: Modelling ozone fluxes to forests for risk assessment: status and prospects, Annals of Forest Science, 66, 401, URL dx.doi.org/10.1051/forest/2009024, 2009.

Uddling, J., Pleijel, H., and Karlsson, P. E.: Measuring and modelling leaf diffusive conductance in juvenile silver birch, Betula pendula, Trees-Structure And Function, 18, 686–695, 2004.

Verwer, J. and Simpson, D.: Explicit methods for stiff ODEs from atmospheric chemistry, Applied Numerical Mathematics, 18, 413–430, 1995.

Verwer, J. G., Blom, J. G., and Hundsdorfer, W.: An implicit explicit approach for atmospheric transport-chemistry problems, Applied Numerical Mathematics, 20, 191–209, 1996.

Volz, A. and Kley, D.: Evaluation of the Montsouris series of ozone measurements made in the nineteenth century, Nature, 332, 240–242, 1988.

Warneck, P.: Chemistry of the Natural Atmosphere, Academic Press, Inc., San Diego, California, 1988.

Wesely, M. L., Cook, D. R., Hart, R. L., and Speer, R. E.: Measurements and Parameterization of Particulate Sulfur Dry Deposition over Grass, J. Geophys. Res., 90, 2131–2143, 1985.

Wind, P., Tarrasón, L., Berge, E., Slørdal, L., Solberg, S., and Walker, S.-E.: Development of a modeling system able to link hemispheric- regional and local air pollution problems, 2002.

Zander, R., Demoulin, P., and Ehhalt, D.H.and Schmidt, U.: Secular increase of the total vertical column abundance of methane derived from IR solar spectra recorded at the Jungfraujoch station, J. Geophys. Res., 94, 11 029–11 039, d8, 1989a.

Zander, R., Demoulin, P., Ehhalt, D.H.and Schmidt, U., and Rinsland, C.: Secular increase of the total vertical column abundance of carbon dioxide above central Europe since 1950, J. Geophys. Res., 94, 11 021–11 028, d8, 1989b.